


Staggered Magnetic Nanowire Devices for Effective Domain-Wall Pinning in Racetrack Memory

M. Al Bahri,¹ B. Borie,² T.L. Jin,³ R. Sbiaa,^{1,*} M. Kläui,² and S.N. Piramanayagam³

¹*Department of Physics, Sultan Qaboos University, P.O. Box 36, PC 123, Muscat, Oman*

²*Institut für Physik, Johannes Gutenberg-Universität Mainz, Staudinger Weg 7, 55128 Mainz, Germany*

³*Division of Physics and Applied Physics, School of Physical and Mathematical Sciences, Nanyang Technological University, Singapore*

 (Received 5 August 2018; revised manuscript received 21 December 2018; published 8 February 2019)

Domain-wall memory devices, in which the information is stored in nanowires, are expected to replace hard disk drives. A problem that remains to be solved in domain-wall memory is to pin the domain walls in a controllable manner at the nanometer scale using simple fabrication. We demonstrate the possibility to stabilize domain walls by making staggered nanowires. Controllable domain-wall movement is exhibited in permalloy nanowires using magnetic fields where the pinning field is about 10 mT. The pinning field and stability of the domain walls can be increased by adjusting the offset dimensions of the staggered nanowires. Domain-wall velocities of about 200 m/s are computed for the experimentally used permalloy nanowires. Domain-wall velocities are found to be independent of pinning strength and stability, providing a way to tune the pinning without compromising domain-wall velocities.

DOI: [10.1103/PhysRevApplied.11.024023](https://doi.org/10.1103/PhysRevApplied.11.024023)

I. INTRODUCTION

Recently, magnetic domain-wall propagation in nanowires has been the subject of intensive investigations [1–18] because of its fundamental characteristics in nanomagnetism and potential applications. For instance, domain-wall-based devices have been proposed for high capacity storage [9,10,15,18], microwave generators [19–25], logic devices [2,3,7,8,26,27], and sensing applications [11,28,29]. The motion of a domain wall (DW) can be driven by a magnetic field or a spin-polarized current [30]. In many of these applications, however, controlling the domain-wall dynamics and its position within the nanowire is crucial. For high-density domain-wall-based memory, several issues regarding the device performance such as thermal stability, power consumption, and operation speed need to be solved. Thermally stable recorded data require keeping DWs at a precise position within the nanowire for a certain period, which could be a period of a few years if the data are archived. Artificial nanowires (NW) with naturally formed defects of different geometries acting as trapping sites have also been investigated using both numerical simulation and experimental observations [4,31–33]. Several studies have also reported that experimentally creating notches using lithography helps to block or pin DWs [5,6,34–41]. These artificial constrictions work as pinning sites for DWs due to their higher pinning potential than that of other pinning sites such as

defects in the NWs. In their work, Bogart *et al.* reported that domain-wall pinning is sensitive to the wall type and its chirality spin structure [31]. Benganza *et al.* investigated domain-wall pinning in (Fe,Co)Cu nanowires grown by electroplating in alumina templates [36]. They demonstrated the possibility to control DWs by applying an external magnetic field. There are also other proposals to use nongeometrical approaches, such as local modification of magnetic properties, to pin DWs [42,43]. Here, we propose and experimentally demonstrate a scheme in which the domain-wall-pinning strength is precisely controlled using an alternative concept of staggered nanowires. The proposed scheme has several advantages. First of all, the proposed scheme is easy to fabricate as it involves two simple wires, which are partially overlapping at the edges. Second, as we will show later, the pinning strength can be easily adjusted by changing the depth of step (d) and length of step (l). Furthermore, this device can be made into a multiple-bit-per-cell memory or a domain-wall memory, based on the number of segments, as shown in Fig. 1.

II. SAMPLE FABRICATION AND CHARACTERIZATION

The samples of Ni₈₁Fe₁₉(30 nm)/Ta(5 nm) are deposited on a thermally oxidized Si substrate using dc-magnetron sputtering in a chamber with an argon pressure of 5.7×10^{-3} mbar at a deposition rate of 0.1 nm/s. The hysteresis loop for permalloy thin films is measured by a superconducting quantum interference device (SQUID).

*rachid@squ.edu.om

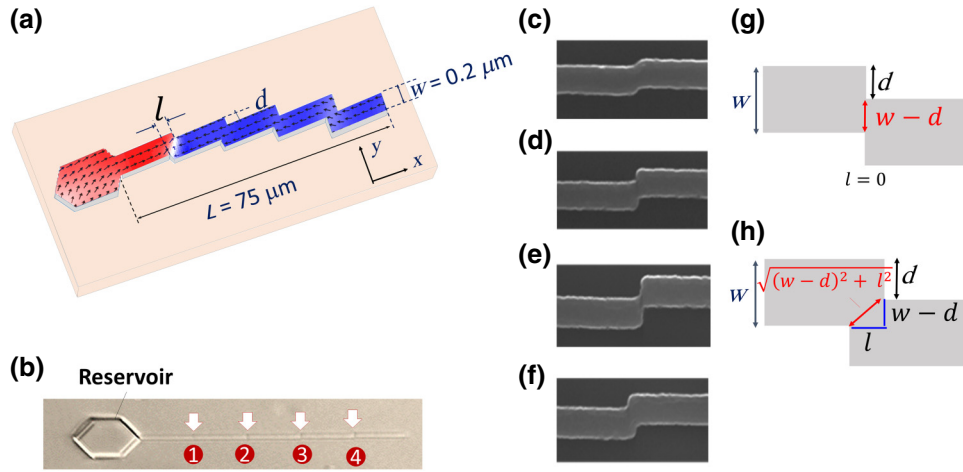


FIG. 1. (a) Schematic representation of the device with multistaggered nanowire. The offset in the x and y directions are defined by l and d , respectively. The large pad is for nucleation of a DW with a smaller magnetic field than the one used for moving it from one pinning region to the other. (b) Optical image of the lithographically fabricated device. The numbers indicate the pinning regions. (c)–(f) SEM images of the devices after electron beam lithography and ion beam etching. The images show wires with different off-set values d and l . (g)–(h) Illustration of a junction of the staggered region with emphasis on the distance between the two corners of the junction. The diagonal, $\sqrt{(w-d)^2 + l^2}$, shown in (h), is related to the pinning strength and the type of domain as will be explained in the simulation part.

Staggered nanowires with a width of 200 nm are patterned by electron beam lithography using a negative resist and ion beam etching. The nanowire is connected to a nucleation pad at one of its ends. Figure 1 shows a schematic of the proposed DW device. As shown in Fig. 1(a), the nanowire has several segments that are offset from each other by a distance d from the previous segment in the y direction. Any segment may also be overlapping with the previous segment in the x direction by a distance l . The DW nanowire in our experiment also has a nucleation pad reservoir at the left end to create domains at lower fields and to avoid the formation of reversed domains in the segments of nanowires. Two types of nanowire are fabricated, that is, nanowires with identical step sizes and nanowires with different values of d and l , as shown in Fig. 6. According to values of d and l , eight nanowires are fabricated having the same stepped area and four nanowires have $l=0$ and $d=50$ nm, 100, 150, and 200 nm. Another four nanowires are fabricated with $l=5$ and $d=5$ nm, 100, 150, and 200 nm.

For the proof-of-concept, we carry out investigations in such geometries based on NiFe. For high-density applications, materials with a perpendicular magnetic anisotropy may be investigated.

III. RESULTS

We show in Fig. 1(b), an optical microscope image of the fabricated device. We can clearly see the reservoir in the optical microscope image. We also show the offset regions in the optical microscope by numbers for

convenience. In Figs. 1(c)–1(f), we show SEM images of offset regions of several devices with different d and l values. We notice that the overlap of the junction region varies as d and l vary, and we will show that the parameters of this region, in particular, the diagonal $\sqrt{(w-d)^2 + l^2}$ shown in Fig. 1(h), determines the pinning strength.

In Fig. 2(a), we show the optical images of one of the preliminary devices based on NiFe (30 nm), which has the same value of l (50 nm) and d (50 nm) at all junctions. To study the pinning effect of such a device, we first saturate the sample in a particular direction with an applied magnetic field of 30 mT. Then, we apply a reversal field in continuous steps of 1 mT until we observe a reversed domain. In Fig. 2(b), we show the formation of such a reversed domain with the application of a reversal field (9 mT). Then, we increase the reversal field further in order to depin the DW from the first junction. However, when the reversal field is about 18 mT, we notice that the DW does not stop at the second junction, but moves rapidly to the end of the nanowire [Fig. 2(c)]. Since the pinning-field strength depends strongly on the values of d and l , and since the values of d and l are uniform at all junctions, they have the same pinning-field strength. Therefore, for an applied magnetic field stronger than the pinning field strength, the DWs are not pinned at the other junctions. These results indicate that this design of staggered nanowires does not allow for controlled pinning at different junctions, in particular when we study the field-driven domain-wall motion.

In the next step, we fabricate 20-nm-thick NiFe-based staggered nanowires with increasing values of d from left

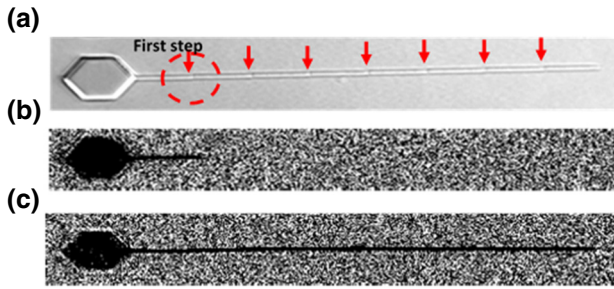


FIG. 2. (a) An optical image of the fabricated device showing the reservoir magnetic area where the DW is first created. The arrows show the different staggered regions where a DW can be stabilized or pinned. In this case, d and l are the same in each step. (b),(c) Two magneto-optical images for the device where the DW is pinned at the first step (b) then moved to the end of the device (c).

to right, by keeping the value of l fixed in the nanowires. We also fabricate several nanowires with various values of l . Figure 3(a) shows the microscopic image and magneto-optical Kerr effect (MOKE) images for nanowires with step dimensions of $l = 0$ nm and various d values (the positions of the steps are indicated by arrows). From Fig. 3(a), we can see that the first domain forms at a field of 9 mT. The DW is pinned at the first junction until a reversal field of 16 mT is applied. The domain wall moves to the next junction only at a reversal field of 21 mT and so on. These results confirm our understanding that the pinning strongly depends on l and d . The improved device design with increasing values of d helps to precisely control the pinning at each junction.

Figure 3(b) shows similar images for nanowires with step dimensions of $l = 50$ nm and various d values. We also notice in this case that the pinning strength and the depinning field depend on the junction as for the nanowire with $l = 0$ nm. However, the depinning field in this case is slightly smaller than that observed with $l = 0$ nm. This can be understood based on the schematics shown in Figs. 1(g) and 1(h). For the case of $l = 0$ nm [Fig. 1(g)], the width of the constriction region is $w - d$, where w is the width of the nanowire. However, for the case of $l > 0$ nm [Fig. 1(h)], the width of the constriction is $\sqrt{(w - d)^2 + l^2}$, which is larger than in the case of $l = 0$ nm. Because the effective constriction is narrower in the case of $l = 0$ nm, it provides the largest pinning field.

We also carry out similar measurements for nanowires with a thicker NiFe layer (30 nm) to understand the effect of thickness. Figure 4 shows the domain observation trend for different values of the reversal magnetic field. We notice that the depinning field is generally larger for thicker NiFe layers (about 30%).

We show in Fig. 4(b) the dependence of the depinning field (H_{dep}) for various values of l and d . We also notice that the H_{dep} increases linearly with d . A similar result is observed for the case of 20-nm-thick permalloy [Fig. 4(c)]. The trend is the same regardless of the values of l . However, for a constant d , the depinning is the largest for $l = 0$ nm. These results are consistent with the schematic shown in Figs. 1(g) and 1(h).

After observing that the staggered nanowire is effective in pinning the DWs, we proceed to examine the stability of the domains formed at the junctions. For this purpose, we use a MOKE set-up observation in the presence of an

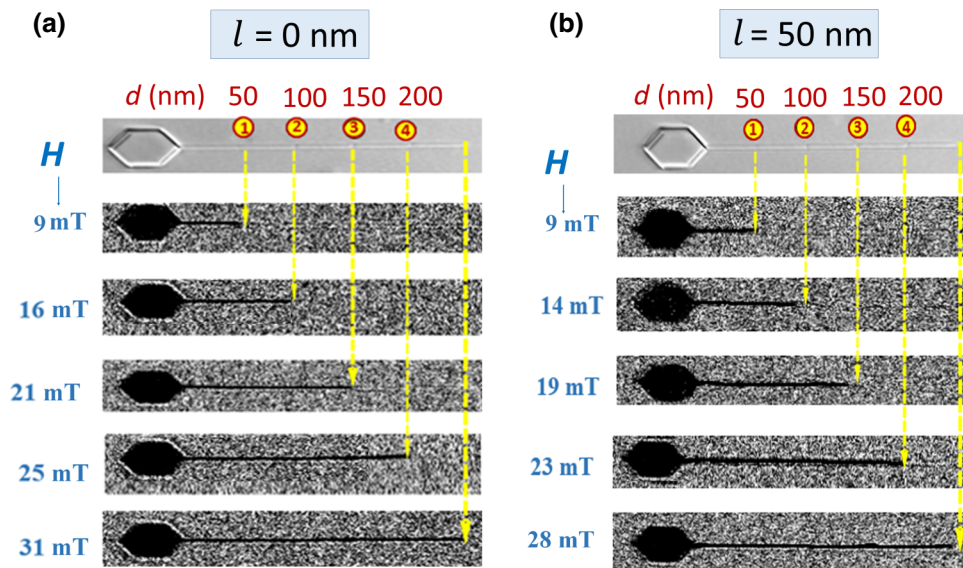


FIG. 3. The fabricated device with (a) $l = 0$ and (b) $l = 50$ nm. The values of d are varied from 50 to 200 nm with a step of 50 nm. The sample is first saturated at 30 mT in one direction then a reversed field is applied in the opposite direction. The depinning field is indicated at the left side of each figure. The length and width of the nanowire are $75 \mu\text{m}$ and 200 nm, respectively.

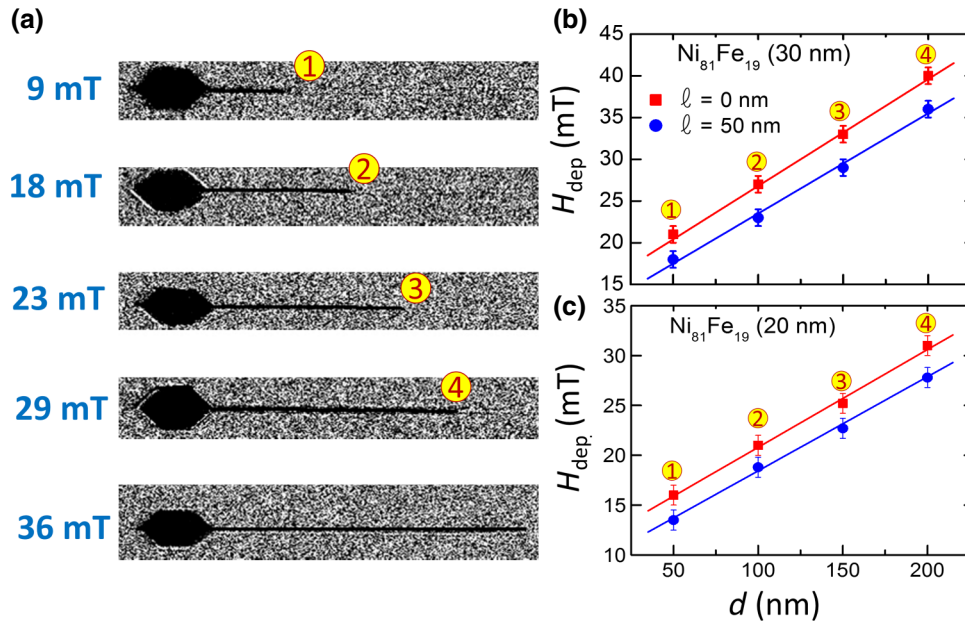


FIG. 4. (a) Magneto-optical images of domain-wall motion for staggered NiFe (30 nm) with $l=0$ and different values of d . The numbers indicate the position of staggered regions where the DW is precisely pinned as the applied magnetic field is increased. The depinning field as a function of d for two different values of l for (b) the case of 30-nm-thick NiFe and (c) for the case of 20-nm-thick NiFe.

in-plane magnetic field. First, we saturate the sample at a magnetic field of 30 mT applied along one direction to saturate the magnetization in that direction. Then, we apply a reversal field and wait for a certain time τ , after which the domain moves. We saturate the sample again, increase the reversal field by 1 mT, and observe the relaxation time for the DW to be displaced from the pinning site. We carry out this investigation of relaxation time (τ) vs the applied reversal magnetic field (H) for values less than that of the depinning field. Figure 5(a) shows the relaxation time τ , for various values of H . We notice that the relaxation time is shorter for larger values of the reversal field and that the values of τ and H follow the relation shown in

Eq. (1) [44–46].

$$\tau = \tau_0' \exp \left[\frac{K_u V}{k_B T} \left(1 - \frac{H}{H_0} \right)^\alpha \right], \quad (1)$$

$$H = H_0 - H_0 \left(\frac{k_B T}{K_u V} \right)^{1/\alpha} \left[\ln \left(\frac{\tau}{\tau_0'} \right) \right]^{1/\alpha}, \quad (2)$$

where τ_0' is the inverse of the attempt time with the value of 10^{-8} s, k_B is the Boltzman constant, and H_0 is the intrinsic depinning field. Equation (1) can be derived to yield Eq. (2). In order to estimate the stability of this device,

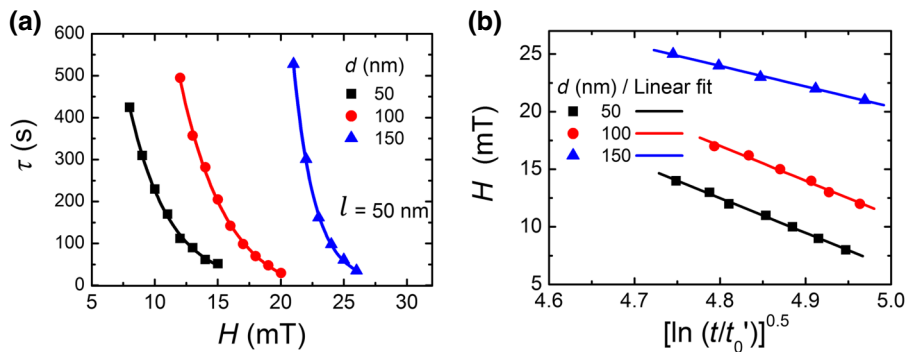


FIG. 5. (a) Relaxation time vs applied magnetic field for staggered nanowires with 30-nm-thick NiFe. For a given applied magnetic field, staggered nanowires with larger d are more stable. (b) The applied magnetic field as a function of relaxation time following Eq. (2) for $\alpha = 1.5$.

TABLE I. Properties obtained from the fit of experimental data to Eq (2), for $\alpha = 1.5$. The values of the three fitting parameters do not differ much with α for $d = 50$ and 100 nm, except for $d = 150$ nm, where an increase can be seen.

Fitting parameters	d (nm)		
	50	100	150
H_0 (T)	0.131	0.135	0.089
$K_u V/k_B T$	27	28.6	37.8
Stability	528 s	2220 s	300 days

we plot H vs $[\ln(\tau/\tau_0')]^{1/\alpha}$, which follows the linear relationship shown in Fig. 5(b). Table I summarizes various properties obtained from the fitting. From the fitted data to Eq. 2, it is found that the domain stability for $d = 150$ nm is about 300 days. For materials with higher anisotropy, the stability could be increased. It is also expected that the stability could be increased by reducing l .

To understand the types of domains formed in these nanowires, we also inspect the magnetic-domain patterns of the samples using a magnetic force microscope (MFM). In Figs. 6(a) and 6(b), we show MFM images of two junctions. We notice a bright spot at the center of the junction in both images, indicating the emergence of the magnetic flux.

However, from the images, it is not clear which type of domain is formed at these junctions. Therefore, we carry out micromagnetic simulations of the junctions for different values of d , using OOMMF [27]. The same material parameters and dimensions as in the experiments are used in the simulation. Four junctions with $l = 50$ nm and $d = 50, 100, 150,$ and 200 nm are simulated. The mesh

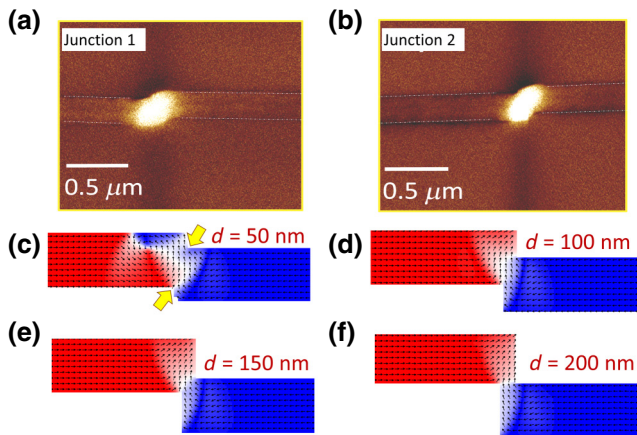


FIG. 6. (a),(b) MFM images of stable DWs at the first and second junctions of staggered NiFe (20 nm). (c)–(f) Micromagnetic simulation images for devices with $l = 50$ nm and different d values. The two yellow arrows indicate the effective width of the junction as described in Fig. 1(h).

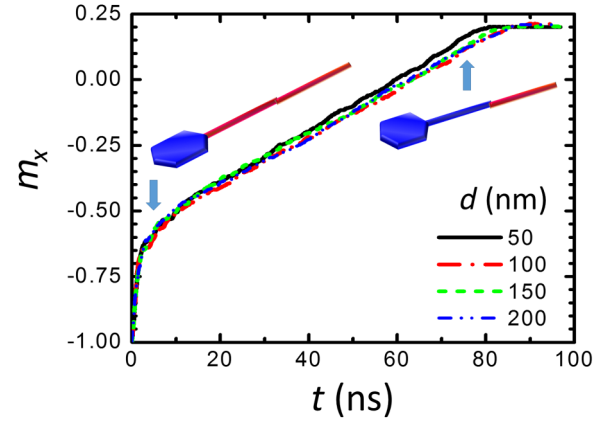


FIG. 7. Normalized x component of NiFe (30 nm) nanowire magnetization as a function of time for devices shown in Figs. 6(c)–6(f). The left bold arrow indicates the position of the DW at the right side of the reservoir and the right bold arrow indicates the position of the DW at the junction region. The DW moves with a constant velocity of about 200 m/s.

size is fixed to $5 \times 5 \times 5$ nm³, sufficiently smaller than the exchange length of NiFe (approximately 5.3 nm). DWs are created at the reservoir first, then depinned in to the nanowire to form domains as shown in Figs. 6(c)–6(f). We notice that the domain-wall type and spin structure formed at the junction depend on the design parameters. For $d = 50$ nm, we observe a vortex DW (VDW). For larger values of d (100 nm and above), a transverse DW (TDW) is observed. The arrows in each graph indicate the magnetic moment directions for the left and right arms, respectively. Snapshot images of the stepped nanowire with different constriction sizes of $l = 50$ nm: (c) $d = 50$ nm, (d) $d = 100$ nm, (e) $d = 150$ nm, and (f) $d = 200$ nm show that the DW is pinned at the stepped area. We also use micromagnetic simulations to estimate the domain-wall velocity. Figure 7 shows the magnetization component (m_x) along the wire direction as a function of time for devices with various values of d . The slope of this graph gives the rate of change of magnetization, or in other words, domain-wall displacement as a function of time. It can be noticed that the slope is almost the same for all the devices. Considering that the length of a nanowire segment is $15 \mu\text{m}$ and that it takes about 70 ns for the DW to cross this distance, we determine the domain-wall velocity to be about 200 m/s, which is in a reasonable range for applications in domain-wall devices as previously shown experimentally [5]. These results also indicate that the domain-wall velocity is independent of d or indirectly of the pinning strength.

IV. SUMMARY

We propose and demonstrate the use of staggered domain-wall nanowires for effective tunable and controlled

pinning of DWs. We have observed the domain-wall movement using MOKE for various applied fields. We find that the domain-wall depinning field (H_{dp}) depends on the design parameters, l and d , and the thickness of the NiFe layer investigated in this work. We also investigate the stability of DWs by relaxation time measurements and notice an exponential dependence between domain-wall relaxation time and the applied magnetic field that allows us to extract stabilities over years for the pinned DWs. In addition, we investigate the domain-wall type by MFM and micromagnetic simulation, and find that the domain-wall type depends on the geometry of the junction. Finally, domain-wall velocities of 200 m/s can be expected for these devices, showing that the combination of fast domain and controlled pinning can lead to good device performance.

ACKNOWLEDGEMENTS

The group in Mainz acknowledges research funding from the European Community under the Seventh Framework Programme—The People Programme, Multi-ITN “WALL” Contract No. 608031 and a European Research Council Proof-of-Concept Grant [No. MultiRev ERC-2014-PoC (665672)], as well as the German Research Foundation (Grant No. SFB TRR173 Spin+X).

- [1] W. Wernsdorfer, B. Doudin, D. Mailly, K. Hasselbach, A. Benoit, J. Meier, J.-Ph. Ansermet, and B. Barbara, Nucleation of Magnetization Reversal in Individual Nanosized Nickel Wires, *Phys. Rev. Lett.* **77**, 1873 (1996).
- [2] D. A. Allwood, G. Xiong, C. C. Faulkner, D. Atkinson, D. Petit, and R. P. Cowburn, Magnetic domain-wall logic, *Science* **309**, 1688 (2005).
- [3] M. P. Kostylev, A. A. Serga, T. Schneider, B. Leven, and B. Hillebrands, Spin-wave logical gates, *Appl. Phys. Lett.* **87**, 153501 (2005).
- [4] M. Kläui, H. Ehrke, U. Rüdiger, T. Kasama, R. E. Dunin-Borkowski, D. Backes, L. J. Heyderman, C. A. F. Vaz, J. A. C. Bland, G. Faini, E. Cambril, and W. Wernsdorfer, Direct observation of domain-wall pinning at nanoscale constrictions, *Appl. Phys. Lett.* **87**, 102509 (2005).
- [5] G. S. D. Beach, C. Nistor, C. Knutson, M. Tsoi, and J. L. Erskine, Dynamics of field-driven domain-wall propagation in ferromagnetic nanowires, *Nat. Mater.* **4**, 741 (2005).
- [6] M. Hayashi, L. Thomas, C. Rettner, R. Moriya, X. Jiang, and S. S. P. Parkin, Dependence of Current and Field Driven Depinning of Domain Walls on Their Structure and Chirality in Permalloy Nanowires, *Phys. Rev. Lett.* **97**, 207205 (2006).
- [7] A. Khitun, D. E. Nikonov, M. Bao, K. Galatsis, and K. L. Wang, Feasibility study of logic circuits with a spin wave bus, *Nanotechnology* **18**, 465202 (2007).
- [8] T. Schneider, A. A. Serga, B. Leven, and B. Hillebrands, Realization of spin-wave logic gates, *Appl. Phys. Lett.* **92**, 022505 (2008).
- [9] S. S. P. Parkin, M. Hayashi, and L. Thomas, Magnetic domain-wall racetrack memory, *Science* **320**, 190 (2008).
- [10] L. O’Brien, D. E. Read, H. T. Zeng, E. R. Lewis, D. Petit, and R. P. Cowburn, Bidirectional magnetic nanowire shift register, *Appl. Phys. Lett.* **95**, 232502 (2009).
- [11] M. Diegel, S. Glathe, R. Mattheis, M. Scherzinger, and E. Halder, A new four bit magnetic domain wall based multibit counter, *IEEE Trans. Magn.* **45**, 3792 (2009).
- [12] T. H. E. Lahtinen, K. J. A. Franke, and S. van Dijken, Electric-field control of magnetic domain wall motion and local magnetization reversal, *Sci. Rep.* **2**, 258 (2012).
- [13] H. Tanigawa, T. Suzuki, S. Fukami, K. Suemitsu, N. Ohshima, and E. Kariyada, Thickness dependence of current-induced domain wall motion in a Co/Ni multi-layer with out-of-plane anisotropy, *Appl. Phys. Lett.* **102**, 152410 (2013).
- [14] A. Fernandez-Pacheco, L. Serrano-Ramón, J. M. Michalik, M. R. Ibarra, J. M. De Teresa, L. O’Brien, D. Petit, J. Lee, and R. P. Cowburn, Three dimensional magnetic nanowires grown by focused electron-beam induced deposition, *Sci. Rep.* **3**, 1492 (2013).
- [15] R. Sbiaa and S. N. Piramanayagam, Multi-level domain wall memory in constricted magnetic nanowires, *Appl. Phys. A* **114**, 1347 (2014).
- [16] B. Van de Wiele, L. Laurson, K. J. A. Franke, and S. van Dijken, Electric field driven magnetic domain wall motion in ferromagnetic-ferroelectric heterostructures, *Appl. Phys. Lett.* **104**, 012401 (2014).
- [17] J.-S. Kim, M.-A. Mawass, A. Bisig, B. Krüger, R. M. Reeve, T. Schulz, F. Büttner, J. Yoon, C.-Y. You, M. Weigand, H. Stoll, G. Schütz, H. J. M. Swagten, B. Koopmans, S. Eisebitt, and M. Kläui, Synchronous precessional motion of multiple domain walls in a ferromagnetic nanowire by perpendicular field pulses, *Nat. Commun.* **5**, 3429 (2014).
- [18] M. Al Bahri and R. Sbiaa, Geometrically pinned magnetic domain wall for multi-bit per cell storage memory, *Sci. Rep.* **6**, 28590 (2016).
- [19] A. Bisig, L. Heyne, O. Boule, and M. Kläui, Tunable steady-state domain wall oscillator with perpendicular magnetic anisotropy, *Appl. Phys. Lett.* **95**, 162504 (2009).
- [20] G. Gubbiotti, S. Tacchi, G. Carlotti, N. Singh, S. Goolaup, A. O. Adeyeye, and M. Kostylev, Collective spin modes in monodimensional magnonic crystals consisting of dipolarly coupled nanowires, *Appl. Phys. Lett.* **90**, 092503 (2007).
- [21] A. V. Chumak, A. A. Serga, B. Hillebrands, and M. P. Kostylev, Scattering of backward spin waves in a one-dimensional magnonic crystal, *Appl. Phys. Lett.* **93**, 022508 (2008).
- [22] S.-K. Kim, K.-S. Lee, and D.-S. Han, A gigahertz-range spin-wave filter composed of width-modulated nanostrip magnonic-crystal waveguides, *Appl. Phys. Lett.* **95**, 082507 (2009).
- [23] R. Sbiaa and R. Chantrell, Domain wall oscillations induced by spin torque in magnetic nanowires, *J. Appl. Phys.* **117**, 053907 (2015).

- [24] B. Van de Wiele, S. J. Hämäläinen, P. Baláz, F. Montoncello, and S. van Dijken, Tunable short-wavelength spin wave excitation from pinned magnetic domain walls, *Sci. Rep.* **6**, 21330 (2016).
- [25] R. Sbiaa, M. Al Bahri, and S. N. Piramanayagam, Domain wall oscillation in magnetic nanowire with a geometrically confined region, *J. Magn. Magn. Mat.* **456**, 324 (2018).
- [26] K.-S. Lee and S.-K. Kim, Conceptual design of spin wave logic gates based on a Mach-Zehnder-type spin wave interferometer for universal logic functions, *J. Appl. Phys.* **104**, 053909 (2008).
- [27] M. Jamali, J. H. Kwon, S.-M. Seo, K.-J. Lee, and H. Yang, Spin wave nonreciprocity for logic device applications, *Sci. Rep.* **3**, 3160 (2013).
- [28] B. Borie, A. Kehlberger, J. Wahrhusen, H. Grimm, and M. Kläui, Geometrical Dependence of Domain-Wall Propagation and Nucleation Fields in Magnetic-Domain-Wall Sensors, *Phys. Rev. Appl.* **8**, 024017 (2017).
- [29] M. Okuda, Y. Miyamoto, E. Miyashita, N. Saito, N. Hayashi, and S. J. Nakagawa, Detection of current-driven magnetic domains in [Co/Pd] nanowire by tunneling magnetoresistive sensor, *J. Appl. Phys.* **117**, 17D516 (2015).
- [30] O. Boulle, G. Malinowski, and M. Kläui, Current-induced domain wall motion in nanoscale ferromagnetic elements, *Mater. Sci. Eng.* **R72**, 159 (2011).
- [31] L. K. Bogart, D. Atkinson, K. O'Shea, D. McGrouther, and S. Mc Vitie, Dependence of domain wall pinning potential landscapes on domain wall chirality and pinning site geometry in planar nanowires, *Phys. Rev.* **B79**, 054414 (2009).
- [32] K. Xu, D. K. Schreiber, Y. L. Li, B. R. Johnson, and J. McCloy, Effect of defects, magnetocrystalline anisotropy, and shape anisotropy on magnetic structure of iron thin films by magnetic force microscopy, *AIP Adv* **7**, 056806 (2017).
- [33] D. Castilla, M. Maicas, J. L. Prieto, and M. P. J. Proenca, Depinning process of magnetic domain walls in cylindrical nanowires with a chemical constraint, *J. Phys. D-Appl. Phys.* **50**, 105001 (2017).
- [34] D. Petit, A.-V. Jausovec, D. Read, and R. P. J. Cowburn, Domain wall pinning and potential landscapes created by constrictions and protrusions in ferromagnetic nanowires, *J. Appl. Phys.* **103**, 114307 (2008).
- [35] S.-H. Huang and C.-H. Lai, Domain-wall depinning by controlling its configuration at notch, *Appl. Phys. Lett.* **95**, 032505 (2009).
- [36] E. Berganza, C. Bran, M. Jaafar, M. Vázquez, and A. Asenjo, Domain wall pinning in FeCoCu bamboo-like nanowires, *Sci. Rep.* **6**, 29702 (2016).
- [37] A. Ding, I. Will, C. Lu, and Y. B. Xu, Vortex domain wall formation in nanowires with twin pinning sites, *IEEE Trans. Magn.* **48**, 2304 (2012).
- [38] U. Bauer, S. Emori, and G. S. D. Beach, Voltage-controlled domain wall traps in ferromagnetic nanowires, *Nat. Nanotech.* **8**, 411 (2013).
- [39] Y. Gao, B. You, X. Z. Ruan, M. Y. Liu, H. L. Yang, Q. F. Zhan, Z. Li, N. Lei, W. S. Zhao, D. F. Pan, J. G. Wan, J. Wu, H. Q. Tu, J. Wang, W. Zhang, Y. B. Xu, and J. Du, Depinning of domain walls in permalloy nanowires with asymmetric notches, *Sci. Rep.* **6**, 32617 (2016).
- [40] D. Backes, C. Schieback, M. Kläui, F. Junginger, H. Ehrke, P. Nielaba, U. Rüdiger, L. J. Heyderman, C. S. Chen, T. Kasama, R. E. Dunin-Borkowski, C. A. F. Vaz, and J. A. C. Bland, Transverse domain walls in nanoconstrictions, *Appl. Phys. Lett.* **95**, 112502 (2007).
- [41] S. Bhatti, R. Sbiaa, A. Hirohata, H. Ohno, S. Fukami, and S. N. Piramanayagam, 5. Spintronics based Random Access Memory: A Review, *Mat. Today* **20**, 530 (2017).
- [42] T. L. Jin, M. Ranjbar, S. K. He, W. C. Law, T. J. Zhou, W. S. Lew, X. X. Liu, and S. N. Piramanayagam, Tuning magnetic properties for domain wall pinning via localized metal diffusion, *Sci. Rep.* **7**, 16208 (2017).
- [43] I. Polenciuc, A. J. Vick, D. A. Allwood, T. J. Hayward, G. Vallejo-Fernandez, K. O'Grady, and A. Hirohata, Domain wall pinning for racetrack memory using exchange bias, *Appl. Phys. Lett.* **105**, 162406 (2014).
- [44] M. P. Sharrock, Time dependence of switching fields in magnetic recording media, *J. Appl. Phys.* **76**, 6413 (1994).
- [45] H. J. Richter, S. Z. Wu, and R. Malmhall, *IEEE Trans. Magn.* **34**, 1540 (1998).
- [46] S. N. Piramanayagam, Perpendicular recording media for hard disk drives, *J. Appl. Phys.* **102**, 011301 (2007).